Design of equivalent coils for anti-interference testing of heavy current transformers

Y. Gao[a], W. Zhao[a], K. Qu[b], H. Li[c], H. Shao[d], Q. Wang[e] and S. Huang[a]
[a]*Department of Electrical Engineering, Tsinghua University, 100084, Beijing, China*
[b]*Beijing Internet Aided Engineering, Ltd, 100083, Beijing, China*
[c]*China Electric Power Research Institute, 430074, Wuhan, China*
[d]*National Institute of Metrology, 100029, Beijing, China*
[e]*School of Engineering and Computing Sciences, Durham University, DH1 3LE, Durham, UK*

Abstract. Heavy current transformers (HCTs) for large generators are intensively interfered by the stray magnetic field produced by heavy adjacent currents, and therefore, anti-interference testing is a crucial process to assure the robustness of HCT products. However, the generation of the interference involves multiphase heavy currents, which are difficult to produce in testing environments, and equivalent testing coils have become an emerging solution to the testing. In this paper, an improved parameter determination algorithm is proposed for the traditional two-segment testing coil configuration, and furthermore, a novel multi-segment testing coil configuration is proposed for better equivalence of the multiphase interference. The effectiveness of the two configurations are thoroughly analyzed by FEM-based simulations as well as physical experiments.

Keywords: Electromagnetic interference, heavy current transformers, partial coil, magnetic shielding, testing.

1. Introduction

Heavy current transformer (HCT) is a key equipment for the monitoring and controlling of large generators, which play important roles in power grids with growing electricity demands. However, as the rated current of generators can reach as large as 40 kA, HCTs equipped on generator bus-bars are intensively interfered by a stray magnetic field produced by adjacent multiphase bus-bars [1-5]. The strong stray field causes a partial magnetic saturation in the HCT iron core, consequently causing measurement error [6-7] or even permanent damage.

This phenomenon brings two challenges to the application of HCTs: the shielding of the stray field, and the anti-interference testing of HCT products. In past studies, several magnetic shielding solutions have been proposed [2-4, 8-10], among which shielding coils are most widely applied in recent products. There are many designs of the shielding coils, e.g., the coil segments can be placed with or without a zimuthal overlapping, and the coils can be either separated or connected to the secondary winding [8]. But the common point is that the total

equivalent number of turns equals zero, so the coils do not affect the working flux, but only produce a non-uniform interfering flux in the core, which can be used to attenuate the stray field.

The development of anti-interference testing of HCT products are facing more difficulties: it is very hard to simulate the real stray field of a large generator in laboratory environments, because this intensive field is the result of some multi phase, extremely high currents. In [11], a method is proposed to simplify the multi-phase interference into a stray field produced by a single large current, but still a large current source as well as bulky bus-bars are required in the testing [12-14]. On the other hand, the principle of shielding coils can also be applied, i.e., introducing a set of partial testing coils to generate an equivalent interfering magnetic field. The method is referred to as "Non-uniformly Distributed Ampere-turns Method" [11], where the testing coils need much lower current to work and thus significantly ease the difficulty of the testing.

Although the principle of the testing coils is clear, it remains an issue to properly optimize these coils, without which the simulated interfering field will not resemble the real stray field, and the testing will not be convincing. Previous works are mostly based on finite-element analysis (FEA) or experiments [4-5, 15], which are accurate enough, but not efficient enough for such optimization-oriented analysis. In [11], an equivalent circuit method is used to determine the parameters of the testing coils, but the highly-simplified model is insufficient to certify a full-range magnetic equivalence in the core.

For a high computation time and high accuracy analysis, an analytical flux model is required. There have been attempts to build a mathematical model of the stray field [1, 12], and in a recent study [16], the mathematical models of the leakage field produced by coils are also derived. The models have been verified on a 30 kA HCT by physical experiments. As these models are crucial to the following analysis, the equations are given here, shown in (1) and (2).

$$\Phi_s = \frac{\mu_0 k_s h i_0}{\pi} \sum_{k=1}^{\infty} \frac{b^k}{k \cdot c^k} \cos(k\varphi) \tag{1}$$

$$\Phi_e = \frac{\mu_0 k_e h i_0}{\pi} \sum_{k=1}^{\infty} \frac{d^k}{k \cdot a^k} \cos(k\varphi) \tag{2}$$

Where μ_0 is the vacuum permeability, k_s and k_c are the core-pickup factors for calibration, h denotes the height of the core, and the definition of the other symbols are given in the diagram shown in Fig. 1.

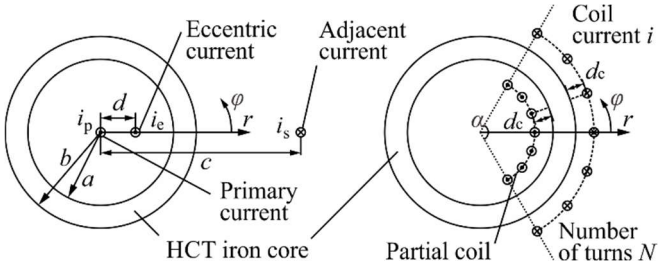

Fig. 1. 2D model of the HCT

The core-pickup factors for mainstream HCTs are calculated by empirical equations shown in (3) and (4).

$$k_s = 1.0123\frac{\sqrt{b^2-a^2}}{h} - 6.6071\sqrt{b^2-a^2} - 0.2300\frac{\sqrt{b-a}}{h} - 0.2258\frac{\sqrt{b+a}}{h} + 3.2412\sqrt{b-a} - 3.2171\sqrt{b+a} - 0.0453\frac{1}{h} - 0.3716 \tag{3}$$

$$k_c = k_s\left(-\frac{3d_c^2}{(a+b)^2} + \frac{3d_c}{2(a+b)} + \frac{3}{25\pi}\alpha + 1\right) \tag{4}$$

Based on the mathematical models, this paper proposes two designs of partial coils for the anti-interference testing of HCTs. Note that in real situations, bus-bars have finite length with turnings or cascading assemblies at the end of the conductors, which will lead to an extra interfering field similar to those produced by adjacent bus-bars [3, 15]. This paper only deals with the cases where the turning of bus-bars are relatively far away from HCT, so that the effect of turning can be neglected. However, if the turning of bus-bars are close to HCT, resulting a notably different interfering flux, it would be necessary to firstly acquire a more accurate model on the flux (either theoretical or numerical), before taking the rest of the steps to design equivalent testing coils.

The paper is organized as follows. In section 2, an improved design method for the two-segment testing coil presented in [11] is introduced. Then, a new multi-segment testing coil

configuration is proposed in section 3. Sections 4 and 5 analyze the equivalence of the testing coil by finite element analysis and physical experiments, respectively, followed by discussions in section 6.

2. Two-segment testing coil configuration

The two-segment testing coil design is firstly proposed in [11], as shown in the right diagram of Fig. 2.

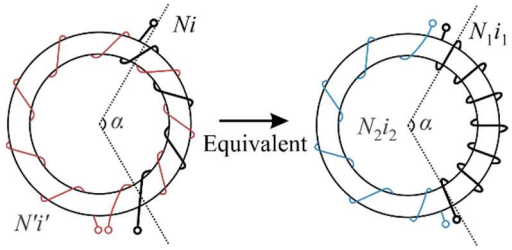

Fig. 2. Partial coils used in the new testing method

This configuration is equivalent to the design shown in the left diagram, where the single partial coil produces the whole leakage magnetic field, and the other coil offsets the working magnetic field. The equivalent condition between the two configurations is

$$\begin{cases} Ni = N_1 i_1 - \dfrac{\alpha}{2\pi - \alpha} N_2 i_2 \\ I_1 = N_1 i_1 + N_2 i_2 = Ni + N'i' \end{cases} \tag{5}$$

Where I_1 denotes the primary current. In turn, when designing the parameters of the coils, one can firstly make an assumption that the leakage magnetic field is exclusively generated by the one partial coil to acquire α and $N'i'$, and then solve $N_1 i_1$ and $N_2 i_2$ by (5).

In a typical, large capacity generator, a total of six bus-bars, respectively three phases and their opposites, are arranged as shown in Fig.3.

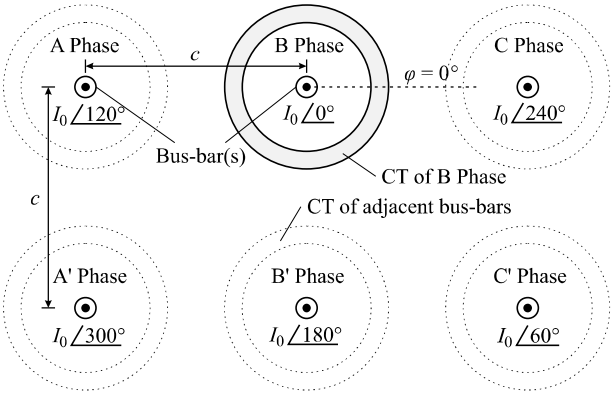

Fig. 3. Typical layout of six-phase bus-bar at terminal of large capacity generator

Among the HCTs of the different phases, the HCT of phase B, along with the HCT of phase B' at a symmetrical position, suffers the most intensive magnetic interference [2], and this is the interference that all HCT products are required to sustain. Therefore, in the anti-interference testing of HCTs, the stray field of the phase B HCT is usually taken as the criterion.

According to [11], the total interfering magnetic field of the phase B HCT in Fig. 3 is equivalent to the stray field produced by a bus-bar locating at phase C and carrying a 0.866 time of rated current. Therefore, if the leakage flux produced by the testing coil resembles the stray flux produced by such a bus-bar, it will also be equivalent to the real magnetic interference.

However, it is impossible to make a perfect equivalence between the stray and the leakage fluxes, because the Fourier series in their equations have different convergence rates. Nevertheless, it is still possible to make a close approximation of the equations, that is, an acceptable equivalence between the real stray magnetic field and the experimental leakage magnetic field. The approximation degree of the flux functions can be determined by the integration of the square of their error, that is, the L2-norm of the flux error function, as shown in (6).

$$\begin{aligned} \|\Phi_c\|^2 &= \frac{1}{2\pi}\int_0^{2\pi}(\Phi_c-\Phi_s)^2 \mathrm{d}\varphi \\ &= \frac{\mu_0^2 h^2 k_s^2}{2\pi^2}\sum_{k=1}^{\infty}\left(\frac{I_0 b^k}{k\cdot c^k}-\frac{4 i_{cs} b^k}{\alpha k^2 (b+d_c)^k}\cdot\sin\frac{k\alpha}{2}\right) \end{aligned} \tag{6}$$

Where the winding current (i), winding turns (N) and the core-pickup factor k_{cs} are expressed as i_{cs} together for convenience, as shown in (7).

$$i_{cs} = k_{cs} N i \tag{7}$$

The purpose of this study is to find the winding angle α as well as the current i_{cs} that can realize the minimum L2-norm for the given HCT and adjacent current. For the sake of clarity, a function $f(\alpha, i_w)$ is introduced to eliminate the constant term of the L2-norm in (8), and the optimal α^* and i_{cs}^*, which minimize the L2-norm, will satisfy

$$f(\alpha^*, i_{cs}^*) = \frac{2\pi^2}{\mu_0^2 h^2 k_s^2} \|\Delta\Phi\|^2 \big|_{\alpha=\alpha^*,\, i_{cs}=i_{cs}^*} = \min_{\alpha,\, i_{cs}} f(\alpha, i_{cs}) = \min_{\alpha} \min_{i_{cs}} f(\alpha, i_{cs}) \tag{8}$$

So far, the original problem has been transformed into 2 steps, each of which is a single variable minimal optimization problem. Each term of the series in $f(\alpha, i_{cs})$ is a quadratic polynomial of i_{cs}. Therefore, the full function can also be broken down into a quadratic function of i_{cs}, as shown in (9).

$$f(\alpha, i_{cs}) = f_1(\alpha) \cdot i_{cs}^2 + f_2(\alpha) \cdot i_{cs} + f_3 \tag{9}$$

Where f_1 and f_2 are functions of α, whereas f_3 is a constant, as shown in (10).

$$\begin{cases} f_1(\alpha) = \dfrac{16}{\alpha^2} \displaystyle\sum_{k=1}^{\infty} \frac{b^{2k}}{k^4 (b + d_c)^{2k}} \sin^2 \frac{k\alpha}{2} \\ f_2(\alpha) = -\dfrac{8 I_0}{\alpha} \displaystyle\sum_{k=1}^{\infty} \frac{b^{2k}}{k^3 c^k (b + d_c)^k} \sin \frac{k\alpha}{2} \\ f_3 = I_0^2 \displaystyle\sum_{k=1}^{\infty} \frac{b^{2k}}{k^2 c^{2k}} \end{cases} \tag{10}$$

According to the properties of quadratic functions, the solution of the first step of optimization is

$$\min_{i_{cs}} f(\alpha, i_{cs}) = f\left(\alpha, -\frac{f_2(\alpha)}{2 f_1(\alpha)}\right) = -\frac{f_2^2(\alpha)}{4 f_1(\alpha)} + f_3 \tag{11}$$

Then, the only remaining problem is the single variable optimization. Since f_3 is a constant, the optimal winding angle α should satisfy

$$-\frac{f_2^2(\alpha^*)}{4 f_1(\alpha^*)} = \min_{\alpha} \left(-\frac{f_2^2(\alpha)}{4 f_1(\alpha)}\right) \tag{12}$$

Numerical solutions of (12) are accessible with the application of computers. Empirically, the winding angle α is limited to a range of 90–180°, where the objective function usually has no more than one minimum point. Such a feature helps simplify the numerical computation.

Finally, when α is determined, the optimal i_{cs}^* will be

$$i_{cs}^* = -\frac{f_2(\alpha^*)}{2f_1(\alpha^*)} \tag{13}$$

3. Multi-segment testing coil configuration

The configuration in Section 2 simplifies multiphase interference into a single phase, which inevitably brings some extra error. In fact, as the analytical model of the stray flux is available, the equation of the multi phase interfering magnetic flux can be acquired. For convenience, the sinusoidal interfering flux is divided into a real part and an imaginary part:

$$\mathrm{Re}(\dot{\boldsymbol{\Phi}}_{\Sigma s}(\varphi)) = \frac{\sqrt{2}\mu_0 k_s h I_0}{\pi} \sum_{k=1}^{\infty} \{\frac{b^k}{k} \cdot \cos(k\varphi + \frac{k\pi}{2}) \cdot [\frac{1}{c_1^k}\cos\frac{k\pi}{2} + \frac{1}{c_2^k} - \frac{1}{c_3^k}\cos(k\theta_c)]\} \tag{14}$$

$$\mathrm{Im}(\dot{\boldsymbol{\Phi}}_{\Sigma s}(\varphi)) = \frac{\sqrt{6}\mu_0 k_s h I_0}{\pi} \sum_{k=1}^{\infty} \{\frac{b^k}{k} \cdot \cos(k\varphi + \frac{k\pi}{2}) \cdot [\frac{1}{c_1^k}\sin\frac{k\pi}{2} - \frac{1}{c_3^k}\sin(k\theta_c)]\} \tag{15}$$

Where

$$\theta_c = \arctan\frac{c_1}{c_2} \tag{16}$$

$$c_3 = \sqrt{c_1^2 + c_2^2} \tag{17}$$

Commonly, the imaginary part is the dominant one, approximately twice as intensive as the real part. Equation (15) shows that the imaginary part of the interfering flux is bilaterally symmetric. Based on this symmetry, a multi-segment testing coil configuration is designed, as presented in Fig.4.

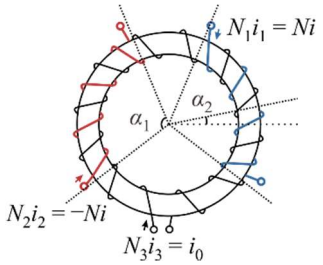

Fig. 4. Diagram of multi-segment testing coil

Both of the two partial coils, symmetrically distributed on the HCT core, have a winding angle of α_1, with a bias positioning angle of α_2. The total ampere-turn of each partial coil is Ni, and as the two coils are in opposite winding directions, the total ampere-turn of the two coils is

zero. d_c denotes the distance between the coil conductor and the HCT core surface. A third uniformly distributed coil is dedicated to generating the working flux and produces no interference in the core.

According to (2), the total leakage flux produced by the two coils $\Phi_{\Sigma c}(\varphi)$ is

$$\Phi_{\Sigma c} = \frac{4\mu_0 k_c h N i}{\pi \alpha_1} \sum_{k=1}^{\infty} \frac{b^k \sin(k\alpha_1/2)}{(b+d_c)^k \cdot k^2} \cdot [\cos(k(\varphi-\alpha_2)) - \cos(k(\varphi-\pi+\alpha_2))] \tag{18}$$

which can be simplified into

$$\Phi_{\Sigma c} = \frac{8\mu_0 k_c h N i}{\pi \alpha_1} \sum_{k=1}^{\infty} \frac{b^k}{(b+d_c)^k \cdot k^2} \cdot \sin\frac{k\alpha_1}{2} \cdot \sin(\frac{k\pi}{2}+k\alpha_2) \cdot \sin(k\varphi+\frac{k\pi}{2}) \tag{19}$$

To make the coil leakage flux equivalent to the real interfering flux, equation (19) should be close to (15). Since the first few Fourier series play the dominant role in both equations, the aim of the design will be to make the first few series in the equations equal to each other.

Usually d_c is limited by the testing environment, and only three parameters, α_1,α_2 and Ni, can be freely adjusted. Consequently, three equations can be listed based on the equivalence of the first three series, and the three variables can be solved. The equation set is listed as follows:

$$\begin{cases} \frac{k_{cs} N i}{\alpha_1} \cdot \sin\frac{\alpha_1}{2} \cdot \cos\alpha_2 = C_1 \\ \frac{k_{cs} N i}{\alpha_1} \cdot \sin\alpha_1 \cdot \sin(2\alpha_2) = C_1 \\ \frac{k_{cs} N i}{\alpha_1} \cdot \sin\frac{3\alpha_1}{2} \cdot \cos(3\alpha_2) = C_3 \end{cases} \tag{20}$$

whereC_1,$C_2$and $C_3$are constants as defined in (21).

$$\begin{cases} C_1 = \frac{\sqrt{3} i_0}{8} \cdot (b+d_c) \cdot (\frac{1}{c_1} + \frac{1}{c_3}\sin\theta_c) \\ C_2 = \frac{\sqrt{3} i_0}{4c_3^2} \cdot (b+d_c)^2 \cdot \sin(2\theta_c) \\ C_3 = \frac{3\sqrt{3} i_0}{8} \cdot (b+d_c)^3 \cdot (\frac{1}{c_1^3} + \frac{1}{c_3^3}\sin(3\theta_c)) \end{cases} \tag{21}$$

The solution of (20) can be acquired by a very simple numerical calculation, and an iteration method is recommended to be applied here. Typically, α_2 is a small value below 20°. Therefore, it can be firstly assumed that α_2 = 0°, based on which α_1, Ni and a new α_2 are successively solved. Then, the updated $\alpha_2$is used in another round of iterations, and after several circulations, the numerical result of α_1,α_2 and Ni can finally be solved.

4. Numerical simulation analysis

4.1. Equivalence of magnetic interference

To perform a simulation analysis, a 30kA HCT sample is selected, whose parameters are given in Table 1.

Table 1
Parameters of 30 kA HCT sample products

Part	Parameter	30 kA HCT
Core	Outer radius a (m)	0.38
	Inner radius b (m)	0.415
	Height h (m)	0.025
Shielding coils	Number of turns N_b	686
	Distance between conductor and core surface d_b (m)	0.02
Adjacent bus-bars	Position c_1 and c_2 (m)	1.2
	Rated current I_0 (A)	30000
Testing coil	Distance between conductor and core surface d_c (m)	0.0575
	Thickness of coil conductor t_c (m)	0.02

According to Sections 2 and 3, the two-segment testing coil and the multi-segment testing coil for this sample are respectively designed, as presented in Table 2.

Table 2
Parameters of designed two-segment testing coil and multi-segment testing coil

Parameter	30 kA HCT	
	Two-segment	Multi-segment
Winding angle α_1	122.1°	75.1°
Positioning angle α_2	-	13.9°
First segment ampere-turns N_1I_1 (A)	14183	2479
Second segment ampere-turns N_2I_2 (A)	15817	−2479
Third segment ampere-turns N_3I_3 (A)	-	30000

Finite element method-based (FEM-based) three-dimensional analysis models of the multi-phase adjacent bus-bars, a two-segment testing coil and a multi-segment testing coil are respectively built in ANSYS. To evaluate the equivalence of magnetic interference, the shielding coils are removed from the analysis. The simulation result of the FEM-based analysis is illustrated in Fig.5 and Fig. 6.

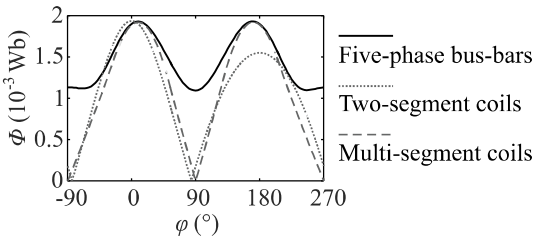

Fig. 5. Simulation result of interfering flux

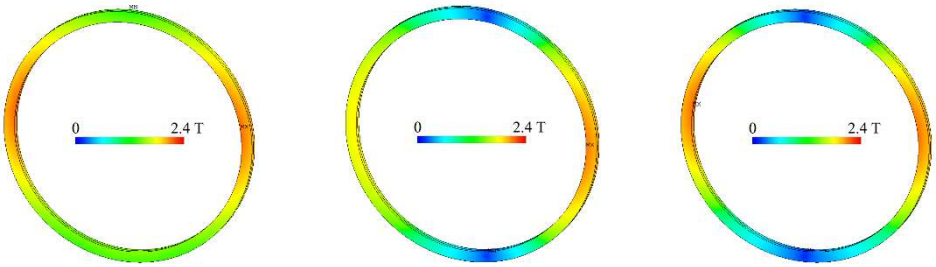

a) b) c)

Fig. 6. Simulation result of interfering magnetic field. (a) Five-phase bus bars; (b) Two-segment coils; (c) Multi-segment coils

Compared to the leakage flux of the two-segment testing coil, the leakage flux of the multi-segment testing coil is evidently closer to the five-phase stray flux, especially in the regions where the stray flux reaches its peak value. The curve of the two-segment testing coil matches around $\varphi = 0°$, but fails to match around $\varphi = 180°$, where another peak occurs.

To conclude, the interference produced by the multi-phase bus-bars is most intensive around $\varphi = 0°$ and $\varphi = 180°$. Both kinds of testing coil can realize an interference with a maximum intensity similar to real situations, but the multi-segment testing coil performs better in simulating an equivalent interference in a wide range.

4.2. Equivalence of remnant magnetic field

In this section, shielding coils are activated in the analysis to verify the equivalence of the remnant magnetic field, i.e., the sum of the interfering field and the field produced by the shielding coils. The diagram of the shielding coils is shown in Fig.7.

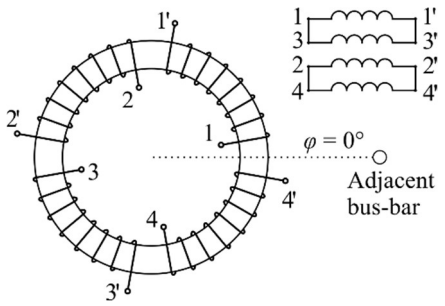

Fig.7. Diagram of shielding coils

The simulation result of the shielding coil currents is listed in Table 3.

Table 3
Simulation result of shielding coil currents

Interfering field	30 kA HCT	
	I_{b1} (A)	I_{b2} (A)
Five-phase stray field	2.77	2.77
Two-segment coil leakage field	2.30	2.30
Multi-segment coil leakage field	2.37	2.37

Under the given three interferences, the currents of the two loops are always the same. Compared to the two-segment testing coil, using the multi-segment testing coil can put the shielding coil current closer to the real interference scenario, but still a significant discrepancy can be observed. This is due to the fact that the real part of the magnetic interference increases the shielding coil current, however the real part is not taken into consideration when designing the testing coil.

The simulation result of the remnant flux is plotted in Fig.8, which indicates that when using the multi-segment testing coil as the equivalent testing equipment, the remnant flux is close to that of the real situation under 360° coverage of the core. The maximum values of the remnant flux $|\Phi_r|_{max}$ are also approximately the same. When using the two-segment testing coil as the equivalent testing equipment, the remnant flux is close to that of the real situation only when $\varphi = -60° \sim 60°$. In other regions, an evident discrepancy can be observed. Moreover, $|\Phi_r|_{max}$ is also lower, although not very significantly, than the value in the real situation.

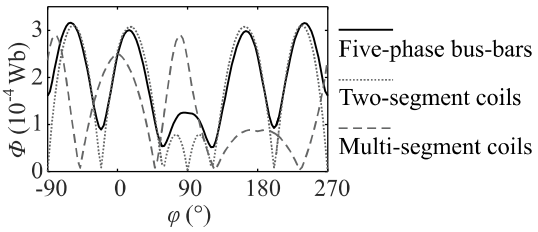

Fig.8. Simulation result of remnant flux

5. Physical experiments

As a three-phase heavy current is difficult to implement in the laboratory environment, a lower-rated 5kA HCT sample is selected for the experiment to reduce the required output current of the power source. The parameters of the sample are given in Table 4.

Table 4
Parameters of 5kA HCT sample product for experiment

Parameter	Value	Parameter	Value	Parameter	Value
Ratio	5000/5A	Inner radius	325 mm	Core inner radius	355mm
Standard accuracy class	0.2 S	Outer radius	455 mm	Core outer radius	430 mm
Number of turns of shielding coils	337	Height	50 mm	Core height	20 mm

As the mathematical models of the interfering fields, which is the basis of the methodology, have been validated on higher-rated 30 kA HCT [16], we believe the conclusions of the experiment can also be expanded to HCTs with higher current rating.

The first part of the experiment is to measure the multi-phase bus-bar interference, a diagram of which is shown in Fig.9. Single turn, 10×120mm^2 cross-section copper bus-bars are applied in the experiment. The adjacent distances c_1 and c_2 are all set to 700mm. The length of the bus-bar l is set to 4000mm, which is long enough to be approximated as infinite. In order to lower the output current, a 3000μF capacitor is connected in parallel to the primary side of the power transformer to compensate for the reactive power.

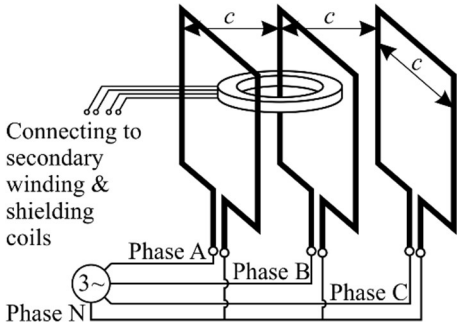

Fig. 9. Spatial diagram of three-phase experiment

The schematic diagram of the B phase testing circuit is shown in Fig.10. For phases A and C, the circuit is the same, except that no HCT sample is put into the circuit.

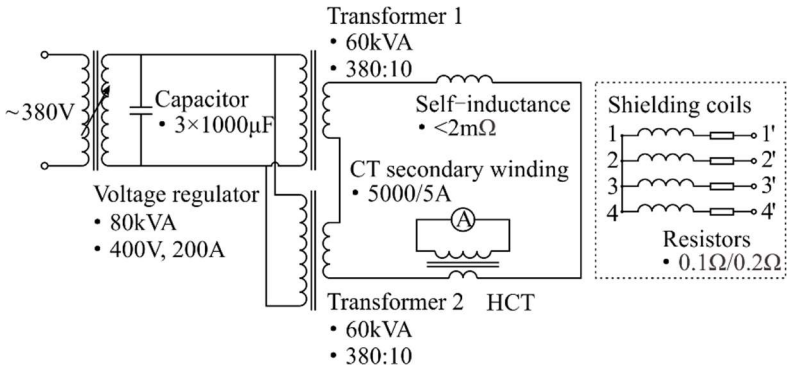

Fig. 10. Schematic diagram of B phase experiment circuit

Fig.11 shows the diagram of the second part of the experiment, which is to measure the interference produced by the equivalent testing coil.

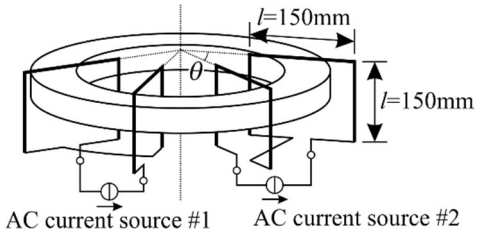

Fig. 11. Diagram of equivalent testing coil experiment

The wires are wound on a 150×150mm^2 epoxy bracket for a fixed distance between the conductor and the core surface d_c of 5.6cm. A total of fifteen brackets are used, which are evenly distributed along the ring of the HCT sample.

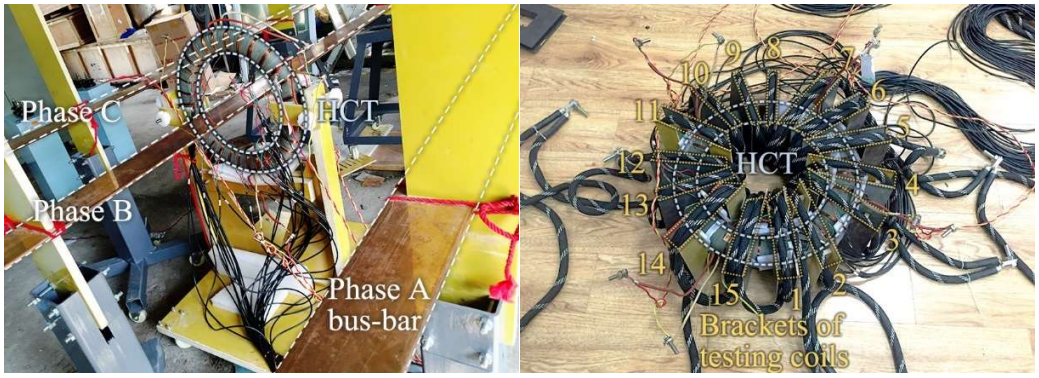

a) b)

Fig. 12. Photographs of physical experiment. (a) Three-phase experiment; (b) Equivalent testing coil experiment

As the position of brackets restricts the winding angle, the parameters of the testing coil are slightly modified based on the optimal design through the methods introduced in sections 3 and 4, and the final parameters are shown in Table 5.

Table 5
Parameters of designed two-segment testing coil and multi-segment testing coil for experiment

Parameter	Two-segment	Multi-segment
Winding angle α_1	120°	75°
Positioning angle α_2	-	6°
First segment ampere-turns N_1I_1 (A)	2450	755
Second segment ampere-turns N_2I_2 (A)	2550	-755
Third segment ampere-turns N_3I_3 (A)	-	5000

The experiment results along with the simulation results are plotted in Fig.13. A significant discrepancy to the previous plot (Fig.5) can be observed: the measured stray flux value at φ= 0° is larger than - rather than equal to -the value at φ= 180°. This is due to the fact that for the lower-rated 5 kA HCT, the stray field is generally weak, so the working flux is more significant, which biases the imaginary part of the stray field. Note that the working flux does not couple with the shielding coils and does not influence the other part of the theoretical analysis.

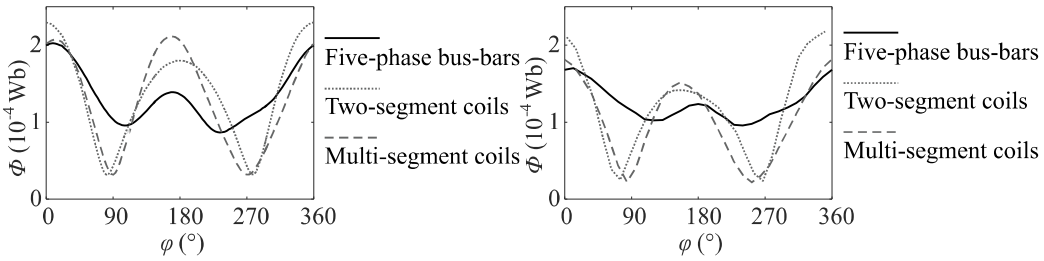

Fig. 13. Interfering flux of 5 Ka HCT. (a) Simulation result; (b) Experimental result

Fig.13 also indicates that both of the two leakage fluxes are close to the multi-phase stray flux around the peak points (φ= 0° and 180°). When making a comparison, it is easy to conclude that the leakage flux produced by the multi-segment testing coil is the more equivalent one, suggesting that the multi-segment testing coil performs better in simulating the real interference than the two-segment testing coil.

In addition, a small phase shift is visible between the curves in Fig. 13. There are several potential causes of the phase shift, including wrong positioning of the measurement coils, deviation of the testing coils, and error of the reference azimuthal point. To mitigate that phase shift, higher accuracy testing equipment is required for the positioning of testing coils.

When the shielding coils are activated, the simulation and the experiment results of the maximum shielding coil current I_{b_max} and the maximum remnant flux $|\Phi_r|_{max}$ are listed in Table 6. Compared to the two-segment testing coil, the multi-segment testing coil has smaller equivalent errors in both I_{b_max} and $|\Phi_r|_{max}$, suggesting that that multi-segment testing coil configuration is the superior one for the anti-interference test of HCT.

Table 6

Simulation and experiment results of I_{b_max} and $|\Phi_r|_{max}$

Interference source	I_{b_max} (A)		$\|\Phi_r\|_{max}$ (10^{-5} Wb)	
	Simulation	Experiment	Simulation	Experiment
Adjacent bus-bars	1.150	1.425	6.11	7.65
Two-segment testing coil	0.838 (−27%)	0.886 (−38%)	5.56 (−9%)	5.17 (−32%)
Multi-segment testing coil	0.846 (−26%)	1.055 (−25%)	5.63 (−8%)	7.16 (−6 %)

Another advantage of the multi-segment testing coil is that the partial coils and the uniformly distributed coil are completely decoupled, and, consequently, the output currents of

the two power sources will not be affected by each other, so the interference and the primary current can be adjusted freely. In the two-segment testing coil configuration, however, as the two coils are magnetically coupled to each other, it is not practical to respectively connect a power source to each coil and adjust the current independently. Instead, the two coils must be connected in series, powered by a single source, and the ratio of N_1I_1 and N_2I_2 is solely decided by the number of turns N_1 and N_2. Such restrictions will introduce burdensome work to change the number of turns when multiple primary current and interference conditions are required to be tested.

6. Conclusions

Based on the mathematical models of the interfering magnetic field in HCT cores, this paper has discussed two testing coil configurations for the anti-interference testing of HCTs. The two-segment testing coil configuration is improved by a more accurate parameter determination algorithm; the multi-segment testing coil configuration is newly proposed in this paper, which is more equivalent to the real multiphase interference. Simulation and experiment studies indicate that both configurations are able to simulate the real multiphase interference of HCTs. Furthermore, among the two types of coil, the novel multi-segment testing coil configuration shows a better equivalence degree.

On the other hand, it is physically impossible to achieve a perfect equivalence between the leakage flux produced by the testing coil and the stray flux encountered by HCTs, since the latter is the result of several phases of currents, whereas the former is, due to limitations of the testing environment, usually powered by single-phase current sources. Moreover, some non-ideal factors in experiments and practical applications, such as positioning error, and bus-bar turnings, cannot ably influence the equivalent performance of testing coils. The authors are still working on building an advanced experiment platform with better accuracy and power capacity, so that tests for higher-rated HCT as well as other types of CT can be performed, and the equivalence error caused by all kinds of factors can be further examined. Additionally, it is worth noting that the slight error in the interfering flux may cause some deviation in the current

of the shielding coils, and the remnant flux -which is the difference between the interfering flux and the shielding flux -can differ significantly. This fact also suggests that it is of great importance to make the interfering flux of the testing environment as close to the real interference as possible.

References

[1] R. A. Pfuntner, The accuracy of current transformers adjacent to high-current busses, *AIEE Trans*, **70** (1951), 1656–1662.

[2] S. Seely, Effect of stray flux on current transformers, *J Sci Technol*, **37** (1970), 115–120.

[3] K. W. Jones, Addressing window type transformer proximity error, *Proc. of 59th Annual Conference on Protect Relay Engineering*, College Station, Texas, USA, (04-06 April 2006), 90-102.

[4] K. Draxler, R. Styblikova, V. Rada, et al, Using a Current Loop and Homogeneous Primary Winding for Calibrating a Current Transformer, *IEEE Transactions on Instrumentation and Measurement*, **62**(6) (2013), 1658–1663. DOI: 10.1109/TIM.2012.2228073.

[5] J. Letosa, A. Uson, J. S. Artal, et al, Uncertainties associated with current measurements: Analysis by the finite element method, *International Journal of Applied Electromagnetics and Mechanics*, **19** (2004), 159–164.

[6] M. Soinski, W. Pluta, S. Zurek, et al, Metrological attributes of current transformers in electrical energy meters, *International Journal of Applied Electromagnetics and Mechanics*, **44** (2014), 279–284. DOI: 10.3233/JAE-141790c.

[7] M. Moghimi Haji, B. Vahidi and S. H. Hosseinian, Current transformer saturation detection using Gaussian mixture models, *Journal of Applied Research & Technology*, **11** (2013), 79–87.

[8] Z. Gajic, S. Holst, D. Bonmann, et al, Stray flux and its influence on protection relays, *Proc. of 65th Annual Conference for Protective Relay Engineers*, College Station, Texas, USA,(02-05 April 2012),425-435.

[9] M. Imamura, M. Nakahara, T. Yamaguchi, et al, Analysis of magnetic fields due to three-phase bus bar currents for the design of an optical current transformer, *IEEE Transactions on Magnetics*, **34**(4) (1998), 2274–2279, Jul. 1998. DOI: 10.1109/20.703866.

[10] H. Y. Yu, J. S Yuan, and J. Zou, Design of novel structure current transformer with shielding coils for overcoming the saturation of core, *IEEE Transactions on Magnetics*, **42**(4) (2006), 1431–1434. DOI: 10.1109/TMAG.2006.872478.

[11] K. Qu, W. Zhao, B. Jiang, et al, New testing method of the shielding effect of heavy current transformer with shielding coils, *IEEE Transactions on Instrumentation and Measurement*, **60**(3) (2011), 839–845. DOI: 10.1109/TIM.2009.2036495.

[12] H. Shao, J. Wu, F. Lin, et al, Effects of stray magnetic fields on the iron core of DCC, *Proc. of Conference on*

Precision Electromagnetic Measurement (CPEM), Washington, DC, USA, (July 2012), 492–493. DOI: 10.1109/CPEM.2012.6251018.

[13] K. Qu, W. Zhao, B. Jiang, et al, Eccentric bus-bar testing method of the shielding effect of a heavy current transformer with shielding coils, *IEEE Transactions on Instrumentation and Measurement*, **61**(1) (2012), 84–92. DOI: 10.1109/TIM.2011.2160913.

[14] J. Xing, W. Zhao, S. Huang, et al, Analysis on eccentric bus-bar testing method of heavy current transformer, *Proc. of IEEE Instrumentation and Measurement Technology Conference (I^2MTC)*, Graz, Austria, (13-16 May 2012), 144-147.

[15] H. Givi, J. S. Moghani, Z. M. A. Vakilian, et al, Three dimensional finite element modeling of a current transformer and analyzing its operation under normal condition, *Proc. of IEEE Iranian Conference on Electrical Engineering (ICEE)*, Mashhad, Iran, (14-16 May 2013), 1–4.

[16] Y. Gao, W. Zhao, Q Wang, et al, Modelling and Optimization of Four-Segment Shielding Coils of Current Transformers. Sensors, **17**(6) (2017), 1218. DOI:10.3390/s17061218.